

O-atom transport catalysis by neutral manganese oxide clusters in the gas phase: Reactions with CO, C₂H₄, NO₂, and O₂

Shi Yin, Zhechen Wang, and Elliot R. Bernstein

Citation: *The Journal of Chemical Physics* **139**, 084307 (2013); doi: 10.1063/1.4819059

View online: <http://dx.doi.org/10.1063/1.4819059>

View Table of Contents: <http://aip.scitation.org/toc/jcp/139/8>

Published by the *American Institute of Physics*

COMPLETELY

REDESIGNED!



**PHYSICS
TODAY**

Physics Today Buyer's Guide
Search with a purpose.

O-atom transport catalysis by neutral manganese oxide clusters in the gas phase: Reactions with CO, C₂H₄, NO₂, and O₂

Shi Yin, Zhechen Wang, and Elliot R. Bernstein^{a)}

Department of Chemistry, NSF ERC for Extreme Ultraviolet Science and Technology, Colorado State University, Fort Collins, Colorado 80523, USA

(Received 27 May 2013; accepted 8 August 2013; published online 26 August 2013)

Reactions of CO, C₂H₄, NO₂, and O₂ with neutral Mn_mO_n clusters in a fast flow reactor are investigated both experimentally and theoretically. Single photon ionization at 118 nm is used to detect neutral cluster distributions through time of flight mass spectrometry. Mn_mO_n clusters are generated through laser ablation of a manganese target in the presence of 5% O₂/He carrier gas. A strong size dependent reactivity of Mn_mO_n clusters is characterized. Reactions Mn₂O₅/Mn₃O₇ + CO → Mn₂O₄/Mn₃O₆ + CO₂ are found for CO oxidation by Mn_mO_n clusters, while only association products Mn₂O_{3.5}C₂H₄ and Mn₃O_{5.7}C₂H₄ are observed for reactions of C₂H₄ with small Mn_mO_n clusters. Reactions of Mn_mO_n clusters with NO₂ and O₂ are also investigated, and the small Mn₂O_n clusters are easily oxidized by NO₂. This activation suggests that a catalytic cycle can be generated for the Mn₂O₅ cluster: Mn₂O₅ + CO + NO₂ → Mn₂O₄ + CO₂ + NO₂ → Mn₂O₅ + CO₂ + NO. Density functional theory (DFT) calculations are performed to explore the potential energy surfaces for the reactions Mn₂O_{4.5}/Mn₃O₇ + CO → Mn₂O_{3.4}/Mn₃O₆ + CO₂, Mn₂O₅ + C₂H₄ → Mn₂O₄ + CH₃CHO, and Mn₂O₄ + NO₂ → Mn₂O₅ + NO. Barrierless and thermodynamically favorable pathways are obtained for Mn₂O₅/Mn₃O₇ + CO and Mn₂O₄ + NO₂ reactions. A catalytic cycle for CO oxidation by NO₂ over a manganese oxide surface is proposed based on our experimental and theoretical investigations. The various atom related reaction mechanisms explored by DFT are in good agreement with the experimental results. Condensed phase manganese oxide is suggested to be a good catalyst for low temperature CO oxidation by NO₂, especially for an oxygen rich sample.
 © 2013 AIP Publishing LLC. [<http://dx.doi.org/10.1063/1.4819059>]

I. INTRODUCTION

Catalytic conversion of harmful gases, produced in fossil fuel combustion, such as carbon monoxide and the oxides of nitrogen, is of utmost importance both environmentally and economically. NO₂ is a very corrosive nitrogen oxide and is one of the most dangerous gases related to health and environmental damage.¹ Depending on temperature, NO₂ can attack metal and especially polymer parts in exhaust systems.² Reactions of NO_x + CO are interesting in several areas, including atmospheric chemistry and surface chemistry. While these redox reactions are exothermic (e.g., Δ_rH = −228 kJ mol^{−1} for the process NO₂ + CO → NO + CO₂), they do not occur directly to any measurable extent at either room or elevated temperatures due to activation barriers (e.g., 114 kJ mol^{−1} for the NO₂/CO couple).³ Catalysts are required to reduce these barriers; the specific role played by transition metal complexes in promoting the oxidation of CO by NO₂ was first reported by Feltham and Kriege as early as 1979.⁴

Catalytic oxidation of CO has been studied on various supported^{5–7} and unsupported^{8–12} MnO_x catalysts, due to their superior ability to activate and supply oxygen. These catalysts attract considerable attentions from both academia and industry due to their low cost and environmental compatibility, in contrast to the expensive noble metal (Pt, Rh, and Pd)

catalysts generally used for the removal of exhaust gas from internal combustion engines. Most of the studies of CO oxidation are performed with stoichiometric manganese oxides. In early works, Klier and Kuchynka¹³ and Kanungo¹⁴ found high catalytic activity over bulk MnO₂ at 293 K and 353 K for the reaction CO to CO₂. Liang *et al.*¹⁵ synthesized MnO₂ catalysts with nanorod morphology and found their catalytic activity to change according to α- ≈ δ- > γ- > β-MnO₂ phase. Variations of catalytic activity with sample polymorphism for otherwise identical bulk compositions can only be explained by assuming that the specific surface termination, Mn–O bond strength, and surface stoichiometry are determining factors. For commercially available manganese oxides the following trends of CO oxidation activity (at 523 K) are reported by Ramesh *et al.*¹⁶ and Wang *et al.*¹⁷: MnO ≤ MnO₂ < Mn₂O₃.

The mechanism for CO oxidation on MnO_x surface is still unknown. Determination of the MnO_x active phase for CO oxidation is a great challenge. Currently, two mechanisms, the Mars-van-Krevelen mechanism (MvK) (e.g., CO adsorbs on surface, picks up a surface O, leaves the surface, and O is replaced by gas phase O₂) and the Langmuir-Hinshelwood (LH) mechanism (e.g., both CO and O₂ adsorb on the surface, react as adsorbates, and leave the surface), are generally proposed to be responsible for the CO oxidation on an MnO_x catalysts.^{10,12,18} An Eley-Rideal mechanism is also predicted in which the CO adsorbs to the MnO_x surface and reacts with a gas phase O₂ molecule: such macroscopic mechanisms are

^{a)} Author to whom correspondence should be addressed. Electronic mail: erb@lamar.colostate.edu.

not easily distinguished, and it is challenging to determine which (if any) of the three mechanisms is dominant in the reaction. The relevant mechanism for this reaction system has thus been debated for decades.^{8–11}

Low-temperature, low-cost, and efficient CO oxidation (removal) can solve serious environmental problems caused by CO emission from automobiles, industrial processing, and even cigarette burning. CO oxidation is also important in other areas such as respiratory protection and fuel gas (e.g., C_nH_{2n+2} and H_2) cleanup. Reforming of hydrocarbons is one of the most attractive approaches to produce hydrogen fuel for polymer electrolyte membrane fuel cells (PEMFC); however, the presence of 1 vol.% CO in the hydrogen stream will poison the Pt anode of a fuel cell, thus removal of CO from the reformat stream for PEMFC applications is essential.¹⁹

Recently, atomic/molecular level mechanisms for condensed phase catalytic reactions have been suggested to be accurately modeled and understood through the study of gas phase cluster reactions:^{20–22} reactions of CO and/or NO_2 with various metal oxide clusters (e.g., $Ce_mO_n^-$,²³ $Al_mO_n^{+/-}$,²⁴ $Fe_mO_n^{+/0/-}$,^{25–29} and $V_mCo_nO_x^{+/0/-}$ ^{30–32}) have been reported and related to condensed phase behavior. The high CO oxidation activity of Co_3O_4 , which is one of the most thoroughly studied 3D metal oxides, is frequently related to the simultaneous presence of tetrahedral Co^{2+} and octahedral Co^{3+} sites.^{31,33,34} Similarly, high activity has also been observed for Mn oxides; however, the catalytic oxidation of CO by NO_2 supported by manganese oxide clusters has not been reported to the best of our knowledge, and no such site requirement has ever been claimed to exist for these oxides. This is probably due to the structural flexibility of Mn oxides, which exist in a number of different stoichiometries (as MnO , Mn_2O_3 , Mn_3O_4 , Mn_5O_8 , and MnO_2 along with their polymorphs) and non-stoichiometric phases, with the Mn valence varying smoothly between +4, as in MnO_2 , and +2, as in MnO .¹⁰

In this paper, we present the first study of CO catalytic oxidation by NO_2 over neutral Mn_mO_n clusters. Density functional theory (DFT) calculations and single photon ionization (SPI) techniques are used to investigate the catalytic activity of Mn_mO_n clusters toward oxidation of CO by NO_2 . The experimental results are well interpreted by the calculations. Catalytically active sites and details of the gas phase reaction mechanism are obtained, and related condensed phase catalytic processes for CO oxidation by NO_2 over manganese oxides at a molecular level are proposed. Mn_mO_n clusters are also studied with regard to their oxidation of unsaturated hydrocarbons (e.g., C_2H_4): only adsorption products $Mn_mO_n(C_2H_4)$ are observed and calculated.

II. METHODS

A. Experimental procedures

The experimental setup for laser ablation coupled with a fast flow reactor employed in this work has been described previously in detail.^{35–39} Only a brief outline of the apparatus is given below. Mn_mO_n clusters are generated in a laser ablation source: manganese plasma, ablated from a manganese

foil disk, reacts with oxygen seeded in helium (5% O_2/He) expansion gas. A 10 Hz, focused, 532 nm Nd^{3+} :YAG laser (Nd^{3+} : yttrium aluminum garnet) with ~ 6 mJ/pulse energy is used for the laser ablation. The expansion gas is pulsed into the vacuum by a supersonic nozzle (R. M. Jordan, Co.) with a backing pressure of typically 75 psi. Generated Mn_mO_n clusters react with reactants in a fast flow reactor (i.d. 6.3 mm \times 76 mm), which is directly coupled to the cluster generation channel (i.d. 1.8 mm \times 19 mm). The reactant gases (CO , C_2H_4 , O_2 , and NO_2), with a 10 psi backing pressure, are injected into the reactor by a pulsed general valve (Parker, Series 9). Timing between the Jordan valve and the general valve opening is optimized for the best product yields. The pressure in the fast flow reactor can be estimated ~ 14 Torr for the reaction.²⁸ Reactants and products are thermalized to 300–400 K by collision during the reaction.⁴⁰ An electric field is placed downstream of the reactor in order to remove any residual ions from the molecular beam. The beam of neutral reactants and products is skimmed into a differentially pumped chamber and ionized by a separated vacuum ultraviolet (VUV) laser beam (118 nm, 10.5 eV/photon). The 118 nm laser light is generated by focusing the third harmonic (355 nm, ~ 30 mJ) of a Nd^{3+} :YAG laser in a tripling cell that contains about a 250 Torr argon/xenon (10/1) gas mixture. An MgF_2 prism (Crystaltechno LTD, Russia, 6° apex angle) is placed into the laser beam to enhance separation of the generated 118 nm laser beam from the 355 nm input laser beam. After the near threshold ionization, photoions are detected by a time of flight mass spectrometer (TOFMS).

B. Computational procedures

Calculations of the structural parameters for neutral Mn_mO_n clusters and the reactions of CO, C_2H_4 , and NO_2 with $Mn_2O_{4,5}$ and Mn_3O_7 clusters are performed employing density functional theory. The hybrid B3LYP exchange-correlation functional^{41–43} and a 6-311+G* basis set^{44–46} are used. This choice of the B3LYP/6-311+G* method with moderate computational cost has been tested to provide reasonable results in previous studies on manganese oxide clusters.^{47,48} This approach yields good results in the interpretation of vibrational spectra of manganese oxides.^{49,50} The adopted DFT method also reproduces the experimental bond dissociation enthalpies of OC–O, ON–O, and Mn–O species. The experimental bond dissociation enthalpies of CO_2 , NO_2 , and MnO are 5.52, 3.16, and 4.17 ± 0.43 eV, respectively,^{51–53} and the DFT calculated values for B3LYP/6-311+G* are 5.54, 3.17, and 4.00 eV, respectively. Binding energies between neutral Mn_mO_n and reactants are calculated at different typical association geometries to obtain the lowest energy structures. The calculations for the potential energy surfaces (PESs) of the reactions of CO, C_2H_4 , and NO_2 with various Mn_mO_n clusters involve geometry optimizations of the reactants, intermediates, transition states, and products. Vibrational frequency calculations are further performed to confirm the global minima ground states and transition states, which have zero and one imaginary frequency, respectively. Additionally, intrinsic reaction coordinate (IRC) calculations are carried out to determine that an estimated transition state connects two

appropriate local minima along the reaction pathway. Binding energies are calculated for a few species employing the Basis Set Superposition Error (BSSE) counterpoise correction.^{54,55} these corrections are found to be insignificant at the present level of theory.

III. RESULTS

A. Experimental

Figure 1 presents a typical TOF mass spectrum of neutral manganese oxide Mn_mO_n ($m = 2-13$, $n = 1-21$) clusters generated by laser ablation of a manganese foil into 5% O_2/He carrier gas, and ionized by 118 nm laser radiation. The intense mass peaks for the manganese oxide series are Mn_mO_n ($m, n = 2, 5; 3, 6-8; 4, 7-9; 5, 9-10; 6, 10-12; 7, 10-12; 8, 11-13; 9, 13-15; 10, 15; 11, 16-17; 12, 17-19$). The relatively high Mn_mO_n signal intensities are at $n = 2m + 1$ ($m = 2, 3$), $n = 2m$ ($m = 4-6$), $n = 2m - 3$ ($m = 7-9$), and $n = 2m - 5$ ($m = 10-12$). Mass spectra are similar to the one shown in Figure 1 for O_2 concentrations in the range 1%–10%.

Mass spectra generated from the reaction of small neutral manganese oxide ($Mn_{2,3}O_n$) clusters with CO and C_2H_4 in a fast flow reactor are presented in Figures 2(b) and 2(c), respectively. By way of comparison, Figure 2(a) shows the TOFMS for $Mn_{2,3}O_n$ clusters reacting with pure He in the reaction cell. If pure He gas is added to the reactor cell, all cluster signals decrease in roughly the same proportion due to scattering by the inert gas in the reactor (Figure 2(a)). The mass signal of Mn_2O_5 decreases about 85% after it reacts with CO, and a comparable signal increase for Mn_2O_4 is observed, whereas no apparent signal depletion is observed for $Mn_2O_{2,3}$ under the same conditions. Significant signal depletion of Mn_3O_7 and increase of Mn_3O_6 are also observed after the reaction with CO. These observations suggest the likely

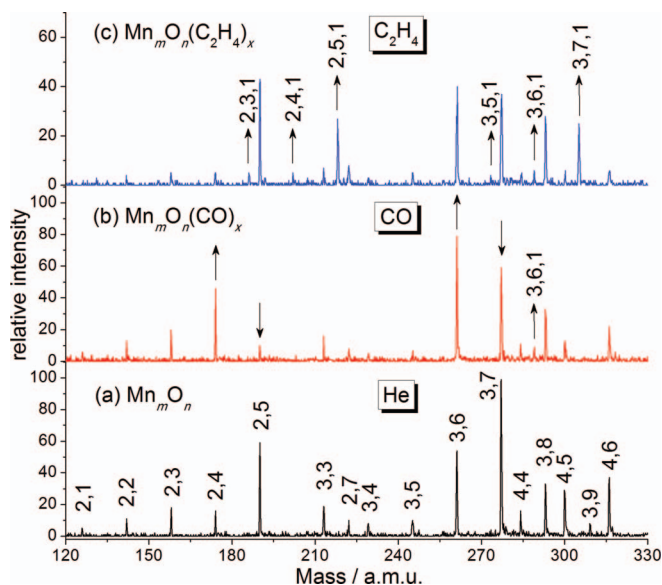


FIG. 2. Neutral manganese oxide cluster distributions after reaction and collision with (a) He, (b) CO, and (c) C_2H_4 in a fast flow reactor. Products are labeled as $Mn_mO_n(M)_x$: m, n, x ($M = CO$ or C_2H_4). See text for details.

reactions, $Mn_2O_5 + CO \rightarrow Mn_2O_4 + CO_2$ and $Mn_3O_7 + CO \rightarrow Mn_3O_6 + CO_2$. The pseudo first order rate constants (k) for the $Mn_mO_n + CO$ reaction in the fast flow reactor can be estimated as previously described,^{28,56} by using the equation $k = \ln(I_0/I)/(\rho \times \Delta t)$, in which I and I_0 are signal magnitudes of the clusters in the presence and absence of H_2 reagent gas, respectively, ρ is the reactant molecular density, and Δt is the reaction time ($\sim 50 \mu s$) in the fast flow reactor. The rate constants $k(Mn_2O_5 + CO)$ and $k(Mn_3O_7 + CO)$ values are estimated to be 6.5×10^{-13} and $1.9 \times 10^{-13} \text{ cm}^3 \text{ molecule}^{-1} \text{ s}^{-1}$, respectively. The absolute error in the values of the rate constants is ca. 30% based on an estimation of ρ and Δt in

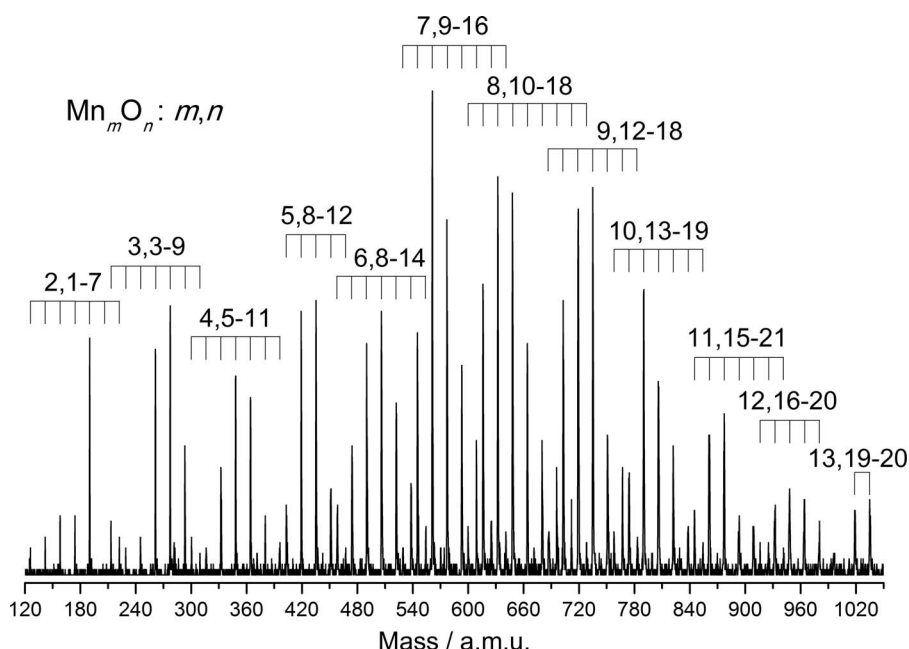


FIG. 1. Neutral manganese oxide Mn_mO_n ($m = 2-13$, $n = 1-21$) distribution detected by 118 nm single photon ionization and time of flight mass spectrometry (SPITOFMS).

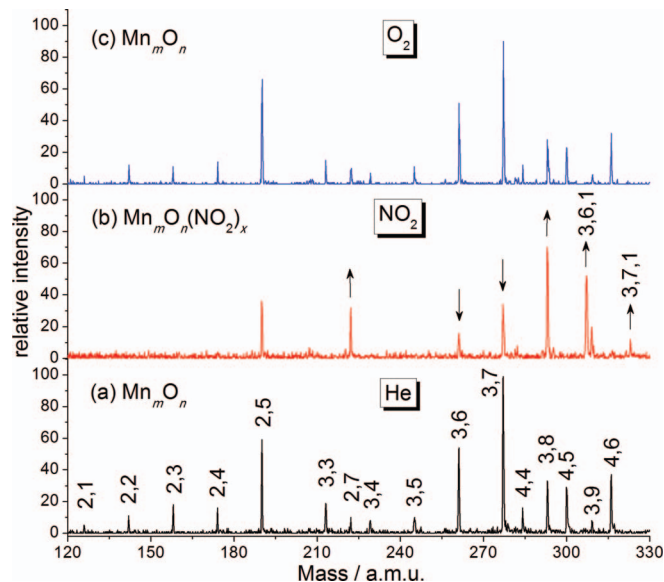


FIG. 3. Neutral manganese oxide cluster distributions after reaction and collision with (a) He, (b) NO_2 , and (c) O_2 in a fast flow reactor. Products are labeled as $\text{Mn}_m\text{O}_n(\text{NO}_2)_x$; m, n, x . See text for details.

the experiments. Reactions of Mn_mO_n clusters with C_2H_4 are also studied (the results are shown in Figure 2(c)) to test the reaction selectivity of small neutral manganese oxide clusters with unsaturated hydrocarbons. The reactivity of neutral $\text{Mn}_{2,3}\text{O}_n$ toward C_2H_4 is quite different from that toward CO: no reactions between $\text{Mn}_{2,3}\text{O}_n$ and C_2H_4 are observed. Only the adduct products $\text{Mn}_2\text{O}_{3,5}\text{C}_2\text{H}_4$ and $\text{Mn}_3\text{O}_{5,7}\text{C}_2\text{H}_4$ (in this mass region) are observed when C_2H_4 is added to the fast flow reactor. Different reaction mechanisms of $\text{Mn}_2\text{O}_{4,5}/\text{Mn}_3\text{O}_7 + \text{CO}$ and $\text{Mn}_2\text{O}_5 + \text{C}_2\text{H}_4$ are interpreted based on quantum chemistry calculations.

In the practical catalytic oxidation of CO by oxidants, the catalysts must be cycled. In order to generate a full catalytic cycle for CO oxidation on manganese oxide clusters, which can play an important role as catalysts, the reactions of Mn_mO_n with oxidants (NO_2 and O_2) are investigated to explore the potential regeneration of catalytically active manganese oxide clusters (Mn_2O_5 and Mn_3O_7) by oxidants. The results of reactions of $\text{Mn}_{2,3}\text{O}_n$ clusters with NO_2 and O_2 in the flow tube reactor are displayed in Figures 3(b) and 3(c), respectively. No reactions between $\text{Mn}_{2,3}\text{O}_n$ and O_2 are observed; however, after reaction with NO_2 , the mass signals of $\text{Mn}_2\text{O}_{1-4}$ disappear completely, and significant signal decrease for Mn_2O_5 and increase for Mn_2O_7 are observed but no association product is observed. This observation suggests possible reactions, $\text{Mn}_2\text{O}_{1-6} + \text{NO}_2 \rightarrow \text{Mn}_2\text{O}_{2-7} + \text{NO}$. The intensities of Mn_3O_n clusters in the presence of NO_2 suggest two different potential reactions: (1) about 70% signal depletion of Mn_3O_6 and the observation of association products $\text{Mn}_3\text{O}_6\text{NO}_2$ with strong intensity suggest the association reaction, $\text{Mn}_3\text{O}_6 + \text{NO}_2 \rightarrow \text{Mn}_3\text{O}_6\text{NO}_2$; and (2) a ca. 70% signal depletion of Mn_3O_7 , a notable signal increase of Mn_3O_8 , and the observation of association products $\text{Mn}_3\text{O}_7\text{NO}_2$ with weak intensity suggest reactions, $\text{Mn}_3\text{O}_7 + \text{NO}_2 \rightarrow \text{Mn}_3\text{O}_7\text{NO}_2/\text{Mn}_3\text{O}_8 + \text{NO}$.

These above experimental results indicate that Mn_2O_5 and Mn_2O_4 clusters are reactive with the CO and NO_2 gas, respectively, and that the Mn_2O_5 cluster could be a catalyst for the CO oxidation by NO_2 . In order to explore and elucidate this mechanistic interpretation, the reaction energies, mechanisms, and potential energy surfaces for the reactions $\text{Mn}_2\text{O}_4 + \text{NO}_2 \rightarrow \text{Mn}_2\text{O}_5 + \text{NO}$ and $\text{Mn}_2\text{O}_5 + \text{CO} \rightarrow \text{Mn}_2\text{O}_4 + \text{CO}_2$ are calculated. Theoretical results can supply more information as discussed in Sec. III B.

B. Theoretical

Figures 4–6 plot the DFT calculated reaction pathways for CO oxidation by Mn_2O_5 , Mn_3O_7 , and Mn_2O_4 , respectively. Mn_2O_5 has a quintet ground state, and the triplet state is above the quintet by 0.55 eV. The Mn_2O_5 cluster contains two bridge-bonded (O_b) and three terminally bonded (O_t) oxygen atoms, and two manganese atoms Mn_I , which bonds with one O_t , and Mn_{II} , which bonds with two O_t . Potential energy profiles for ${}^3,5\text{Mn}_2\text{O}_5 + \text{CO}$ are determined for CO attaching to the different possible sites on the Mn_2O_5 cluster. CO can bond to Mn_I (paths 1 and 2 of Figure 4), O_t on Mn_I (paths 3 and 5 of Figure 4), or O_t on Mn_{II} (paths 4 and 6 of Figure 4). Significant overall reaction barriers (ORB) of 0.54 eV, 0.33 eV, 0.78 eV, 1.23 eV, and 1.34 eV are determined for the reaction paths 2 to 6 for reaction of Mn_2O_5 with CO, respectively. For reaction path 1, the result in Figure 4 shows that no ORB (or negative ORB of -0.11 eV) exists for CO reacting with Mn_2O_5 in the ground state. The negative ORB for the $\text{Mn}_2\text{O}_5 + \text{CO}$ reaction coordinate is consistent with the system high reactivity (Figure 2(b)). Note that, the crossing of spin triplet (path 2) and quintet (path 1) potential energy surfaces (spin conversion⁵⁷) is obtained: this surface path crossing suggests that the initial reactants ${}^3\text{Mn}_2\text{O}_5 + \text{CO}$ can also form intermediate $\text{In}1$ through the spin conversion point (CP) in Figure 4.

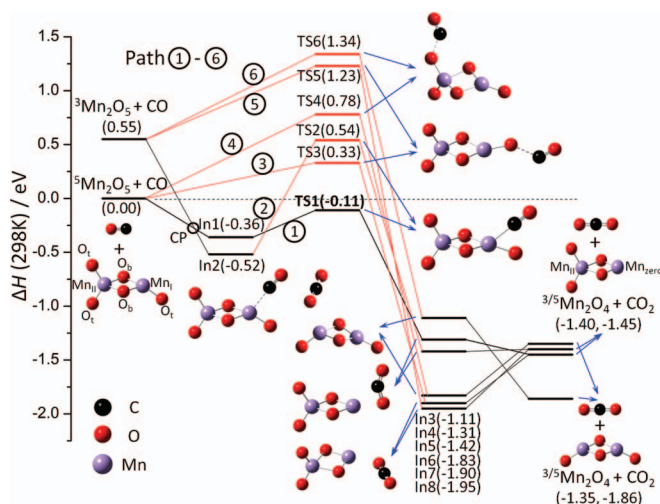


FIG. 4. A potential energy surface profile for the reaction $\text{Mn}_2\text{O}_5 + \text{CO} \rightarrow \text{Mn}_2\text{O}_4 + \text{CO}_2$. Energies are in eV and relative to the initial reactant energy of ${}^5\text{Mn}_2\text{O}_5 + \text{CO}$. Energy levels are calculated by B3LYP/6-311+G*. The spin multiplicity (M) is listed as ${}^M\text{Mn}_2\text{O}_{4,5}$. “CP” denotes a possible spin conversion point for reaction paths 1 and 2. See text for details.

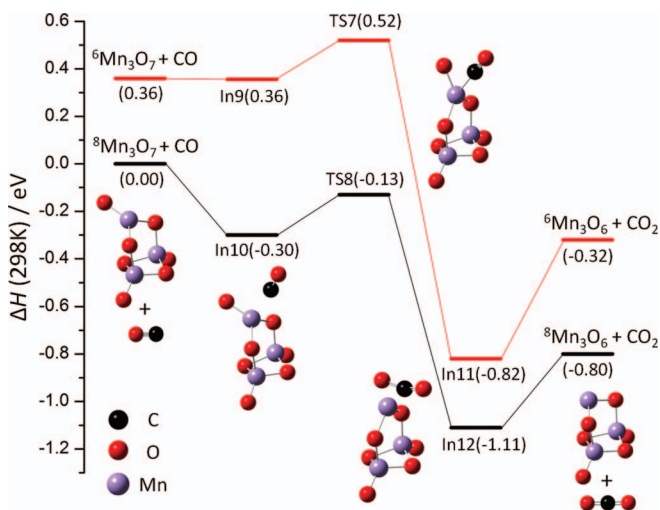


FIG. 5. A potential energy surface profile for the reaction $\text{Mn}_3\text{O}_7 + \text{CO} \rightarrow \text{Mn}_3\text{O}_6 + \text{CO}_2$. Energies are in eV and relative to the initial reactant energy of ${}^8\text{Mn}_3\text{O}_7 + \text{CO}$. Energy levels are calculated by B3LYP/6-311+G*. The spin multiplicity (M) is listed as ${}^M\text{Mn}_3\text{O}_{6,7}$. See text for details.

The DFT calculation summarized in Figure 5 predicts that the Mn_3O_7 has an octet ground state and a sextet state above it at 0.36 eV. A positive ORB of 0.16 eV is present for CO approaching sextet Mn_3O_7 (on Mn_I), whereas the ORB is negative (-0.13 eV) for CO approaching octet Mn_3O_7 (on Mn_I). The reaction pathway shown in Figure 6 predicts that the oxidation of CO by the ground and low-lying excited states of Mn_2O_4 is subject to significant ORBs 0.60 eV and 0.24 eV (even considering a spin inversion mechanism⁵⁷). These DFT results can be used to explain the observed reactivity of Mn_2O_5 , Mn_3O_7 , and Mn_2O_4 clusters.

The PESs and the optimized geometries of reaction intermediates and transition states calculated by DFT for the reaction ${}^5\text{Mn}_2\text{O}_5 + \text{C}_2\text{H}_4 \rightarrow {}^5\text{Mn}_2\text{O}_4 + \text{CH}_3\text{CHO}$ (oxidation of an unsaturated hydrocarbon) are presented in Figure 7. The most stable adsorption structure (In18) is for one C atom of

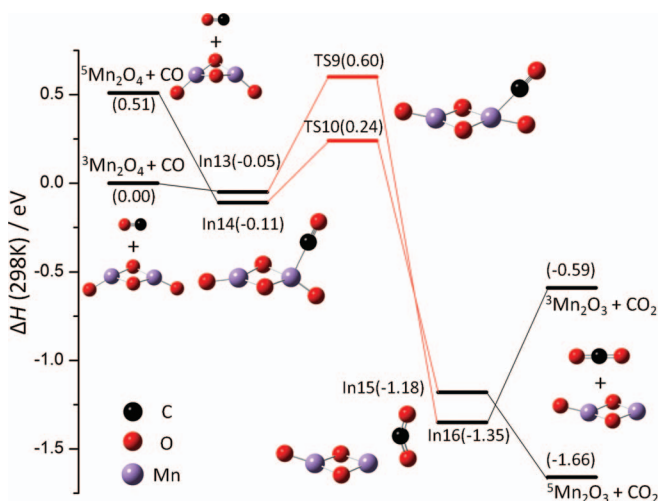


FIG. 6. A potential energy surface profile for the reaction $\text{Mn}_2\text{O}_4 + \text{CO} \rightarrow \text{Mn}_2\text{O}_3 + \text{CO}_2$. Energies are in eV and relative to the initial reactant energy of ${}^3\text{Mn}_2\text{O}_4 + \text{CO}$. Energy levels are calculated by B3LYP/6-311+G*. The spin multiplicity (M) is listed as ${}^M\text{Mn}_2\text{O}_{3,4}$. See text for details.

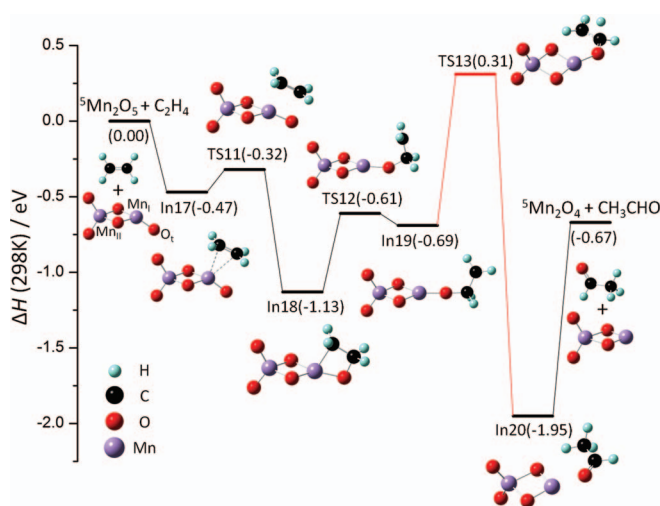


FIG. 7. A potential energy surface profile for the reaction ${}^5\text{Mn}_2\text{O}_5 + \text{C}_2\text{H}_4 \rightarrow {}^5\text{Mn}_2\text{O}_4 + \text{CH}_3\text{CHO}$. Energies are in eV and relative to the initial reactant energy of ${}^5\text{Mn}_2\text{O}_5 + \text{C}_2\text{H}_4$. Energy levels are calculated by B3LYP/6-311+G*. The spin multiplicity (M) is listed as ${}^M\text{Mn}_2\text{O}_{4,5}$. See text for details.

C_2H_4 bonded to manganese atom Mn_I and the other C atom bonded to the oxygen atom O_I of Mn_I in the Mn_2O_5 cluster. A positive ORB of 0.31 eV is present for a hydrogen transfer from the CH_2 moiety bonded to O_I to the other carbon via TS13. The positive ORB and stable association intermediate In18 (-1.13 eV) of the ${}^5\text{Mn}_2\text{O}_5 + \text{C}_2\text{H}_4$ system are consistent with the adsorptive but non-oxidative reactivity of Mn_2O_5 toward C_2H_4 presented in Figure 2(c).

In order to study the regeneration mechanism for the manganese oxide cluster Mn_2O_5 by oxidant NO_2 , DFT calculations are performed for the reaction $\text{Mn}_2\text{O}_4 + \text{NO}_2 \rightarrow \text{Mn}_2\text{O}_5 + \text{NO}$. Cluster ${}^5\text{Mn}_2\text{O}_4$, which is a product of the barrierless reaction path 1 obtained from the calculation results presented in Figure 4 ($\text{O}_{I2}\text{Mn}_{II}\text{O}_{b2}\text{Mn}_{\text{zero}}$, Mn_{zero} : without O_I), and ${}^2\text{NO}_2$ are adopted as initial reactants. Figure 8 presents the reaction pathway for ${}^5\text{Mn}_2\text{O}_4$ oxidized by NO_2 . NO_2 bonds to the Mn_{zero} atom of Mn_2O_4 to form intermediate I21, and the NO moiety transfers to Mn_{zero} via transition state TS14 (-1.04 eV) to yield In22: this structure has an $\text{Mn}_2\text{O}_5(\text{NO})$ geometry with an Mn_INO attachment. The release of NO from the Mn_2O_5 cluster requires 0.18 eV, and then Mn_2O_5 is regenerated from Mn_2O_4 oxidation by NO_2 .

Thus, good agreement between DFT calculations and the experimental observations has been achieved through the above collective mechanism. This agreement between theory and experiment enables us to draw qualitative conclusions concerning the mechanisms of CO oxidation by NO_2 on Mn_mO_n clusters based on the DFT results.

IV. DISCUSSION

A. Mechanisms of CO oxidation by manganese oxide clusters

Special size dependent behavior is identified for the reaction of Mn_mO_n clusters with CO both in experiments and calculations, as presented in Figure 2 and Figures 4–6, respectively. Clusters Mn_2O_5 and Mn_3O_7 are found to have

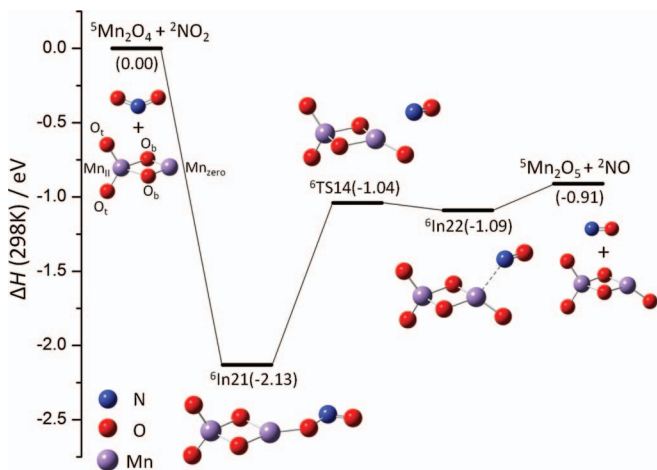


FIG. 8. A potential energy surface profile for the reaction ${}^5\text{Mn}_2\text{O}_4 + 2\text{NO}_2 \rightarrow {}^5\text{Mn}_2\text{O}_5 + 2\text{NO}$. Energies are in eV and relative to the initial reactant energy of ${}^5\text{Mn}_2\text{O}_4 + 2\text{NO}_2$. Energy levels are calculated by B3LYP/6-311+G*. The spin multiplicity (M) is listed as ${}^M\text{Mn}_m\text{O}_n$, ${}^M\text{NO}_x$, ${}^M\text{In}_x$, and ${}^M\text{TS}_y$. See text for details.

high reactivity for CO oxidation. Figure 9 presents the lowest energy structures (with Mn–O bond lengths) found for $\text{Mn}_2\text{O}_{3.5}$ (left panel) and $\text{Mn}_3\text{O}_{6.7}$ (right panel). Only the highest singly occupied molecular orbital (HSOMO) for each of these neutral clusters is shown in Figure 9, the other singly occupied molecular orbitals (SOMOs) are displayed in Figure S1 of the supplementary material.⁵⁸ Two different types of manganese–oxygen bonding are evident: (1) bridged Mn–O–Mn bonding with a Mn–O bond length in the range of 1.76–1.96 Å, and (2) terminal Mn–O bond with a length in the range of 1.55–1.58 Å (the longest terminal Mn–O bond lengths are found in Mn_2O_5 and Mn_3O_7 clusters). Figures 4 and 5 show very similar processes for CO oxidation on Mn_2O_5 and Mn_3O_7 clusters, even though the relative energies of the reaction intermediates and transition states depend on the individual clusters and their spin states. The first step

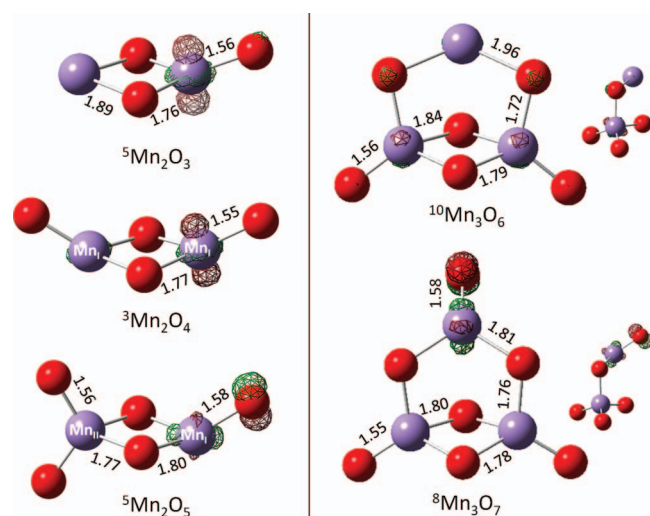
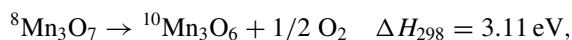
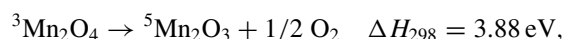
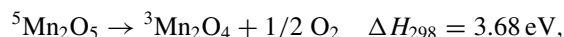


FIG. 9. DFT optimized structures for $\text{Mn}_2\text{O}_{3.5}$ (left panel) and $\text{Mn}_3\text{O}_{6.7}$ (right panel). For each cluster, the lowest energy structure with the HSOMO, bond lengths, and spin multiplicity (M : ${}^M\text{Mn}_m\text{O}_n$) is listed. For $\text{Mn}_3\text{O}_{6.7}$, a second angle view is provided to have a better understanding of the geometry.

in these reactions involves CO adsorption onto the clusters by carbon–manganese interaction to form species $\text{O}_n\text{Mn}_{m-1}\text{Mn}-\text{CO}$. Oxygen manganese interactions ($\text{O}_n\text{Mn}_{m-1}\text{Mn}-\text{OC}$) are also explored: species formed in this way are usually unstable or very high in energy. Direct CO_2 formation (carbon oxygen interaction such as $\text{O}_4\text{Mn}_2\text{O}-\text{CO}$ shown in reaction paths 3–6 in Figure 4) is also tested. The reaction barriers are much higher than the one presented for path 1 (Figure 4). These results suggest that the CO molecule will adsorb on the Mn site. The study of CO oxidation by small iron oxide clusters also finds that the initial intermediate formation involves a carbon iron interaction.²⁸ For the oxidation of CO by anionic AuO_n^- clusters, the initial complex formation involves a carbon oxygen interaction: the CO molecule is able to bind directly to an oxygen atom of AuO_n^- .⁵⁹ This could imply an intrinsic mechanism difference for CO oxidation over noble and non-noble metal catalysts.

After the initial intermediate formation through carbon manganese interactions, the second critical step of the reaction involves one terminal Mn–O_t bond activation. This is clearly demonstrated in Figures 4 and 5 in which the activated Mn–O_t bond lengths (in Å in the list below) of the first transition states are significantly longer than those of the initial intermediates: 1.68 versus 1.59 for ${}^5\text{Mn}_2\text{O}_5 + \text{CO}$; and 1.68 versus 1.58 for ${}^8\text{Mn}_3\text{O}_7 + \text{CO}$. The activation energies, which are 0.25 eV (${}^5\text{Mn}_2\text{O}_5 + \text{CO}$) and 0.17 eV (${}^8\text{Mn}_3\text{O}_7 + \text{CO}$) with respect to the initial intermediates, decide the ORBs of these two reactions. Both active O_t atoms of Mn_2O_5 and Mn_3O_7 are bonded to a Mn_I(IV) atom. The oxidation state of Mn in nanostructured MnO_x , a highly active catalyst for CO oxidation, is determined to be 3.4 ± 0.1 .¹⁰

In order to understand the different reactivity of Mn_mO_n clusters, deoxygenation energies for $\text{Mn}_2\text{O}_{4.5}$ and Mn_3O_7 clusters are calculated and compared to the CO_2 deoxygenation as given in following equations:



The CO_2 deoxygenation energy (5.54 eV) is higher than that of $\text{Mn}_2\text{O}_{4.5}$ and Mn_3O_7 clusters (3.11–3.88 eV), which implies that the oxygenation of CO by these Mn_mO_n clusters should be thermodynamically available. Nevertheless, in the PES for the reaction of the Mn_2O_4 cluster with CO displayed in Figure 6, a high barrier is consistent with the non-oxidative reactivity of Mn_2O_4 , although Mn_2O_4 clusters contain O_t atoms bonded with Mn(IV) sites. As presented in Figure 9, the HSOMO for the triplet Mn_2O_4 (the coupling is antiferromagnetic on two Mn_I sites) is mainly a d -type orbital localized on one Mn_I atom. The HSOMO for the quintet Mn_2O_5 (one unpaired electron (d^1) on the Mn_{II} site and three unpaired electrons (d^3) on the Mn_I site), however, is composed of non-bonding orbitals of Mn_I d atomic orbitals and O_t p atomic orbitals: this Mn_2O_5 orbital localizes on Mn_I

and O_t (bonded with Mn_I) atoms. This implies that the O_t atom (on Mn_I) of Mn_2O_5 is easily activated for the interaction of CO with an Mn_2O_5 cluster. A little longer length of Mn_I-O_t bond in the Mn_2O_5 cluster (1.58 Å compared with 1.55 Å in the Mn_2O_4) also enhances its activity with the carbon atom of the adsorbed CO. The low HSOMO distribution on the O_t atom and a short bond length of the Mn_I-O_t bond of the Mn_2O_4 cluster are both responsible for the high positive ORB of the reaction ${}^3Mn_2O_4 + CO$: the activation energy, 0.65 eV (${}^3Mn_2O_4 + CO$) with respect to the initial intermediates, is much higher than that for reactions ${}^5Mn_2O_5 + CO$ (0.25 eV) and ${}^8Mn_3O_7 + CO$ (0.17 eV).

In summary, our calculational and experimental results indicate that $Mn_I(IV)$ atoms of reactive (catalytic) Mn_2O_5 and Mn_3O_7 clusters are the active sites for holding CO molecules during the CO oxidation processes. The next essential step is the $Mn_I(IV)-O_t$ bond activation, which then transfers the O_t atom to the adsorbed CO to yield the intermediate $Mn_mO_{n-1}(CO_2)$ ($m, n = 2, 5$ and $3, 7$). The catalytic reactivity of Mn_mO_n clusters is found to be associated with the following factors: (1) the presence of a $Mn_I(IV)-O_t$ moiety; (2) the HSOMO distribution on the O_t atom; and (3) the length of the $Mn_I(IV)-O_t$ bond.

Additionally, ethylene is chosen as a prototypical example to consider for the selective oxidative property of Mn_mO_n clusters toward hydrocarbons. Spectra shown in Figure 2(c) make clear that C_2H_4 cannot be oxidized by $Mn_{2,3}O_n$ clusters, as only association products $Mn_2O_{3-5}C_2H_4$ and $Mn_3O_{5-7}C_2H_4$ are observed. A positive ORB (0.31 eV) and stable association intermediate In18 (-1.13 eV) of the ${}^5Mn_2O_5 + C_2H_4$ system are also obtained from DFT calculations (Figure 7): these combined results are consistent with the non-oxidative reactivity of $Mn_2O_5 + C_2H_4$. Taken together with the CO/ NO_2 reactions clarified above, these C_2H_4 results suggest that manganese oxide may be a potential catalyst for CO removal from a hydrocarbon stream, since the selective CO oxidation by the Mn_2O_5 cluster is observed both experimentally and theoretically and is more energetically favorable than the hydrocarbon and Mn_mO_n clusters interaction.

B. The oxidation of Mn_mO_n clusters by oxidants

In the practical catalytic oxidation of CO by oxidants, the catalyst must be involved in a cyclic reaction. Reactions of $Mn_{2,3}O_n$ clusters with NO_2 and O_2 oxidants are investigated to explore the regeneration of oxidative Mn_2O_5 and Mn_3O_7 clusters, and to develop a full catalytic cycle for CO oxidation by oxidants over manganese oxide clusters. As displayed in Figure 3(c), neither association nor reaction between $Mn_{2,3}O_n$ clusters and O_2 occurs. Since the O–O bond breaking process is subject to a high absolute reaction barrier (~ 1.2 eV), based on the study of reactions between small neutral iron oxide clusters and oxygen at low temperature,²⁸ the absence of reaction for $O_2 + Mn_{2,3}O_n$ is proposed to be due to a high barrier for the O–O bond breaking process at low temperature.

As suggested by the results of reactions of $Mn_{2,3}O_n$ with NO_2 (Figure 3(b)), the reaction ($Mn_2O_4 + NO_2 \rightarrow Mn_2O_5 + NO$) is studied by DFT potential energy surface calcula-

tions to understand the regeneration of reactive Mn_2O_5 clusters. The allowed reaction pathway for NO_2 with Mn_2O_4 cluster indicates that NO_2 is adsorbed on the Mn_{zero} atom of a Mn_2O_4 cluster in the first step of the reaction. The lowest energy structure of the association product $Mn_2O_4(NO_2)$ (Figure 8) shows that NO_2 binds with Mn_2O_4 clusters through forming a $MnO_4Mn_{zero}-ONO$ intermediate. These results suggest that the Mn_{zero} atom, generated by the $CO \rightarrow CO_2$ reaction on Mn_2O_5 , is the active site for the adsorption of NO_2 . The next step for Mn_2O_5 regeneration is the rupture of O–NO bond and transfer of the NO moiety to Mn_{zero} , forming In22 (Mn_2O_5-NO) via a low energy transition state TS14 (-1.04 eV). To generate products, only 0.18 eV is required to release NO from In22 to form $Mn_2O_5 + NO$. Based on these DFT calculations, the overall reaction of $Mn_2O_4 + NO_2 \rightarrow Mn_2O_5 + NO$ is barrierless and thermodynamically favorable. The regeneration of Mn_2O_5 from Mn_2O_4 oxidation by NO_2 is readily accomplished.

C. Understanding the catalytic cycle for CO oxidation by NO_2 over manganese oxide at a molecular/atomic level

A Langmuir-Hinshelwood type mechanism between molecular CO and atomic oxygen generating carbon dioxide (CO_2) on the surface of metals or metals supported by oxides is generally accepted, while a Mars-van-Krevelen type mechanism is frequently suggested for pure metal oxides.¹⁰ The LH mechanism proposes two surface adsorbed gas phase species (in this case, CO and NO_2) reacting with one another, and the MvK mechanism proposes one surface adsorbed species (in this case CO) reacting with a gas phase molecule (in this case NO_2): section of these macroscopic mechanism is applicable to the present reaction. The identified mechanism for CO oxidation by NO_2 on the manganese oxide cluster (surface), however, has not been proposed previously. Studies for CO oxidation by Mn_mO_n clusters and Mn_mO_n clusters oxidation by NO_2 in the gas phase aid in the understanding of the related condensed phase catalysis reaction at an atomic level. Catalytic clusters in the gas phase can be seen as a good model system for the active moieties that exist on a catalyst surface. Thereby, a catalytic cycle for CO oxidation by NO_2 on manganese oxide surfaces can be proposed, and is presented in Figure 10. This proposal is offered based on experimental and calculational results presented in Figures 2–5 and 8.

This suggested mechanism generally parallels that proposed by Luo *et al.* for the CO oxidation by O_2 at low temperature (< 220 °C) on the α - Mn_2O_3 nanocatalyst surface.¹⁸ The cluster based mechanism, however, presents additional important information about active sites on the catalyst surface. Our proposed mechanism indicates that the CO molecule adsorbs on the $Mn_I(IV)$ site, which bonds to only one terminal oxygen atom, and reacts with the active O_t atom on that $Mn_I(IV)$ site. The mechanism suggested from condensed phase surface studies does not supply the details of active sites on the catalytic surface.

We conclude that the $Mn_I(IV)$ surface sites are the active sites for adsorption of a CO molecule. The CO attaches to the $Mn_I(IV)$ site through its C atom (Mn–C bond formation

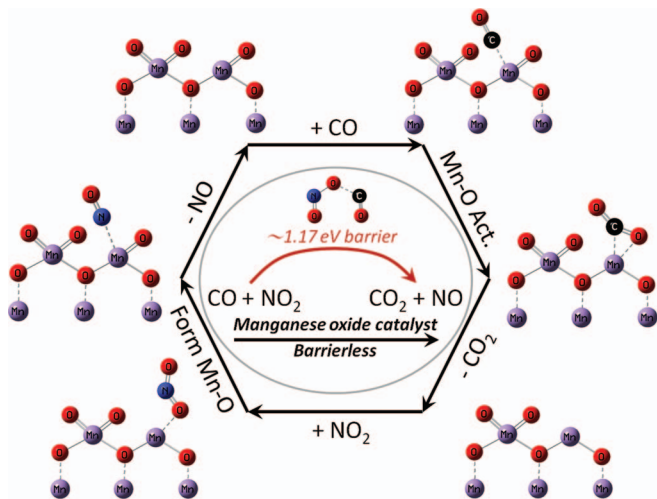


FIG. 10. Possible catalytic cycle for the CO oxidation by NO_2 over manganese oxide catalysts at the molecular level.

is also proposed in Ref. 18). The O_t atom bonded to the same $\text{Mn}_I(\text{IV})$ site is active for oxidation of the adsorbed CO. The CO_2 molecule can be formed through O_t activation and desorbed to the gas phase leaving a bare Mn site on the catalytic manganese oxide surface. A NO_2 molecule from the gas phase can then be adsorbed on the bare Mn site through one of its oxygen atoms. The $\text{Mn}_I(\text{IV})\text{-O}_t$ bond is regenerated via an NO moiety transformation to the Mn site (formation of an Mn-N bond). The formed NO molecule desorbs to the gas phase with the catalytic manganese oxide surface unchanged. The CO oxidation by NO_2 , $\text{CO} + \text{NO}_2 \rightarrow \text{CO}_2 + \text{NO}$ (with a high positive barrier ~ 1.2 eV) is thereby possible over the manganese oxide catalyst surface. The catalytic cycle (depicted in Figure 10) can give a more clear idea of manganese oxide catalyst surface behavior, and therefore is helpful to understand the heterogeneous catalytic reaction mechanism of CO oxidation by NO_2 on the condensed phase catalyst surface. To enhance the catalytic activity of a manganese oxide catalyst, one should try to increase the $\text{Mn}_I(\text{IV})$ sites at the surface.

V. CONCLUSION

Reactions of neutral manganese oxide clusters Mn_mO_n with CO, C_2H_4 , NO_2 , and O_2 are investigated by time of flight mass spectrometry employing 118 nm single photon ionization and DFT calculations. Strong cluster size dependent behavior is observed for the oxidation reactions of CO by Mn_mO_n clusters ($m = 2\text{--}13$, $n = 1\text{--}21$). PESs are calculated for CO oxidation reactions on $\text{Mn}_2\text{O}_{4,5}$ and Mn_3O_7 clusters: CO molecules are predicted to be adsorbed on the $\text{Mn}_I(\text{IV})$ site. Reactions for CO to form CO_2 on Mn_2O_5 and Mn_3O_7 clusters are estimated as overall barrierless and thermodynamically favorable processes. Theoretical calculations suggest that activity of Mn_2O_5 and Mn_3O_7 clusters is related to: (1) a $\text{Mn}_I(\text{IV})\text{-O}_t$ moiety, (2) the HSOMO distribution on the O_t atom, and (3) the bond length of the $\text{Mn}_I(\text{IV})\text{-O}_t$ bond. Two essential steps are present in the oxidation of CO by Mn_mO_n clusters: (1) the initial intermediate formation that in-

volves a carbon-manganese interaction; and (2) the $\text{Mn}_I(\text{IV})\text{-O}_t$ bond activation that determines the overall reaction barrier. The Mn-O bond activation energy at room temperature varies from -0.11 eV (Mn_2O_5) to 0.60 eV (Mn_2O_4). For reactions with C_2H_4 , only association products (such as $\text{Mn}_2\text{O}_5(\text{C}_2\text{H}_4)$ and $\text{Mn}_3\text{O}_7(\text{C}_2\text{H}_4)$) are observed, which suggests that Mn_2O_5 and Mn_3O_7 clusters, which have high activity for the oxidation of CO, adsorb, but do not oxidize small hydrocarbon compounds. In order to generate a whole catalytic reaction cycle for CO oxidation through commonly used oxidants, reactions of Mn_mO_n clusters with NO_2 and O_2 are also investigated. Small Mn_2O_n clusters are easily oxidized by NO_2 , which suggests that the catalytically reactive Mn_2O_5 clusters can be regenerated by NO_2 after reaction with CO: $\text{Mn}_2\text{O}_5 + \text{CO} + \text{NO}_2 \rightarrow \text{Mn}_2\text{O}_4 + \text{CO}_2 + \text{NO}_2 \rightarrow \text{Mn}_2\text{O}_5 + \text{CO}_2 + \text{NO}$. A condensed phase surface catalytic cycle for CO oxidation by NO_2 is proposed based on the present gas phase cluster experimental and theoretical studies. The various reaction mechanisms explored by DFT calculations are in good agreement with the experimental results. The exposed $\text{Mn}_I(\text{IV})$ species with only one terminal oxygen on a manganese oxide surface are predicted to be the active catalytic sites for low temperature catalytic oxidation of CO by oxidants like NO_2 .

ACKNOWLEDGMENTS

This work is supported by a grant from the US Air Force Office of Scientific Research (AFOSR) through Grant No. FA9550-10-1-0454, the National Science Foundation (NSF) ERC for Extreme Ultraviolet Science and Technology under NSF Award No. 0310717, and the National Science Foundation through XSEDE resources under Grant No. TG-CHE110083.

1. S. W. Massey, *Sci. Total Environ.* **227**, 109 (1999).
2. M. S. Li, K. Seshan, and L. Lefferts, *Chin. J. Chem.* **25**, 435 (2007).
3. J. H. Zhang, Y. C. Wang, and Y. L. Leng, *Comput. Theor. Chem.* **1001**, 15 (2012).
4. R. D. Feltham and J. C. Kriege, *J. Am. Chem. Soc.* **101**, 5064 (1979).
5. R. Craciun, B. Nentwick, K. Hadjiivanov, and H. Knözinger, *Appl. Catal., A* **243**, 67 (2003).
6. Y.-F. Han, F. Chen, Z.-Y. Zhong, K. Ramesh, E. Widjaja, and L.-W. Chen, *Catal. Commun.* **7**, 739 (2006).
7. Y.-F. Han, F. Chen, Z. Zhong, K. Ramesh, L. Chen, and E. Widjaja, *J. Phys. Chem. B* **110**, 24450 (2006).
8. C. S. Brooks, *J. Catal.* **8**, 272 (1967).
9. M. I. Zaki, M. A. Hasan, L. Pasupulety, and K. Kumari, *Thermochim. Acta* **311**, 97 (1998).
10. K. Frey, V. Iablokov, G. Safran, J. Osan, I. Sajo, R. Szukiewicz, S. Chenakin, and N. Kruse, *J. Catal.* **287**, 30 (2012).
11. S. Ching, D. A. Kriz, K. M. Luthy, E. C. Njagi, and S. L. Suib, *Chem. Commun. (Cambridge)* **47**, 8286 (2011).
12. V. Iablokov, K. Frey, O. Geszti, and N. Kruse, *Catal. Lett.* **134**, 210 (2010).
13. K. Klier and K. Kuchynka, *J. Catal.* **6**, 62 (1966).
14. S. B. Kanungo, *J. Catal.* **58**, 419 (1979).
15. S. Liang, F. Teng, G. Bulgan, R. Zong, and Y. Zhu, *J. Phys. Chem. C* **112**, 5307 (2008).
16. K. Ramesh, L. Chen, F. Chen, Y. Liu, Z. Wang, and Y.-F. Han, *Catal. Today* **131**, 477 (2008).
17. L.-C. Wang, Q. Liu, X.-S. Huang, Y.-M. Liu, Y. Cao, and K.-N. Fan, *Appl. Catal., B* **88**, 204 (2009).
18. Y. Luo, Y. Q. Deng, W. Mao, X. J. Yang, K. K. Zhu, J. Xu, and Y. F. Han, *J. Phys. Chem. C* **116**, 20975 (2012).

- ¹⁹H. B. Zou, S. Z. Chen, Z. L. Liu, and W. M. Lin, *Powder Technol.* **207**, 238 (2011).
- ²⁰S. Yin and E. R. Bernstein, *Int. J. Mass. Spectrom.* **321**, 49 (2012).
- ²¹M. Schlagen and H. Schwarz, *Catal. Lett.* **142**, 1265 (2012).
- ²²M.-Y. Jia, B. Xu, X.-L. Ding, Y.-X. Zhao, S.-G. He, and M.-F. Ge, *J. Phys. Chem. C* **116**, 9043 (2012).
- ²³X. N. Wu, X. L. Ding, S. M. Bai, B. Xu, S. G. He, and Q. Shi, *J. Phys. Chem. C* **115**, 13329 (2011).
- ²⁴G. E. Johnson, E. C. Tyo, and A. W. Castleman, *J. Phys. Chem. A* **112**, 4732 (2008).
- ²⁵B. V. Reddy, F. Rasouli, M. R. Hajaligol, and S. N. Khanna, *Chem. Phys. Lett.* **384**, 242 (2004).
- ²⁶B. V. Reddy and S. N. Khanna, *Phys. Rev. Lett.* **93**, 068301 (2004).
- ²⁷G. L. Gutsev and C. W. Bauschlicher, *Chem. Phys. Lett.* **380**, 435 (2003).
- ²⁸W. Xue, Z. C. Wang, S. G. He, Y. Xie, and E. R. Bernstein, *J. Am. Chem. Soc.* **130**, 15879 (2008).
- ²⁹J. J. Melko, S. G. Ard, J. A. Fournier, N. S. Shuman, J. Troe, and A. A. Viggiano, *J. Phys. Chem. A* **116**, 11500 (2012).
- ³⁰G. E. Johnson, J. U. Reveles, N. M. Reilly, E. C. Tyo, S. N. Khanna, and A. W. Castleman, *J. Phys. Chem. A* **112**, 11330 (2008).
- ³¹Y. Xie, F. Dong, S. Heinbuch, J. J. Rocca, and E. R. Bernstein, *Phys. Chem. Chem. Phys.* **12**, 947 (2010).
- ³²Z. C. Wang, S. Yin, and E. R. Bernstein, *J. Phys. Chem. Lett.* **3**, 2415 (2012).
- ³³X. Xie, Y. Li, Z.-Q. Liu, M. Haruta, and W. Shen, *Nature (London)* **458**, 746 (2009).
- ³⁴L. Hu, K. Sun, Q. Peng, B. Xu, and Y. Li, *Nano Res.* **3**, 363 (2010).
- ³⁵S. Yin, Y. Xie, and E. R. Bernstein, *J. Chem. Phys.* **137**, 124304 (2012).
- ³⁶S. Yin, Y. Xie, and E. R. Bernstein, *J. Phys. Chem. A* **115**, 10266 (2011).
- ³⁷S. G. He, Y. Xie, F. Dong, S. Heinbuch, E. Jakubikova, J. J. Rocca, and E. R. Bernstein, *J. Phys. Chem. A* **112**, 11067 (2008).
- ³⁸S. G. He, Y. Xie, Y. Q. Guo, and E. R. Bernstein, *J. Chem. Phys.* **126**, 194315 (2007).
- ³⁹S. Yin, Z. C. Wang, and E. R. Bernstein, *Phys. Chem. Chem. Phys.* **15**, 4699 (2013).
- ⁴⁰M. E. Geusic, M. D. Morse, S. C. O'Brien, and R. E. Smalley, *Rev. Sci. Instrum.* **56**, 2123 (1985).
- ⁴¹A. D. Becke, *Phys. Rev. A* **38**, 3098 (1988).
- ⁴²A. D. Becke, *J. Chem. Phys.* **98**, 5648 (1993).
- ⁴³C. T. Lee, W. T. Yang, and R. G. Parr, *Phys. Rev. B* **37**, 785 (1988).
- ⁴⁴V. A. Rassolov, J. A. Pople, M. A. Ratner, and T. L. Windus, *J. Chem. Phys.* **109**, 1223 (1998).
- ⁴⁵R. Krishnan, J. S. Binkley, R. Seeger, and J. A. Pople, *J. Chem. Phys.* **72**, 650 (1980).
- ⁴⁶W. J. Hehre, R. Ditchfield, and J. A. Pople, *J. Chem. Phys.* **56**, 2257 (1972).
- ⁴⁷M.-Y. Jia, B. Xu, X.-L. Ding, S.-G. He, and M.-F. Ge, *J. Phys. Chem. C* **116**, 24184 (2012).
- ⁴⁸G. L. Gutsev, B. K. Rao, and P. Jena, *J. Phys. Chem. A* **103**, 10819 (1999).
- ⁴⁹G. L. Gutsev, B. K. Rao, P. Jena, X. Li, and L.-S. Wang, *J. Chem. Phys.* **113**, 1473 (2000).
- ⁵⁰G. L. Gutsev, B. K. Rao, and P. Jena, *J. Phys. Chem. A* **104**, 11961 (2000).
- ⁵¹S. W. Benson, *J. Chem. Educ.* **42**, 502 (1965).
- ⁵²D. deB. Darwent, *Bond Dissociation Energies in Simple Molecules*, National Bureau of Standards (NSRDS-NBS, Washington, DC, 1970).
- ⁵³J. B. Pedley and E. M. Marshall, *J. Phys. Chem. Ref. Data* **12**, 967 (1983).
- ⁵⁴A. K. Rappe and E. R. Bernstein, *J. Phys. Chem. A* **104**, 6117 (2000).
- ⁵⁵S. F. Boys and F. Bernardi, *Mol. Phys.* **100**, 65 (2002).
- ⁵⁶F. Dong, S. Heinbuch, Y. Xie, J. J. Rocca, and E. R. Bernstein, *J. Phys. Chem. A* **113**, 3029 (2009).
- ⁵⁷D. Schröder, S. Shaik, and H. Schwarz, *Acc. Chem. Res.* **33**, 139 (2000).
- ⁵⁸See supplementary material at <http://dx.doi.org/10.1063/1.4819059> for all singly occupied molecular orbitals (SOMOs) of Mn₂O_{3.5} and Mn₃O_{6.7} clusters in Figure S1.
- ⁵⁹M. L. Kimble, A. W. Castleman, R. Mitrić, C. Bürgel, and V. Bonačić-Koutecký, *J. Am. Chem. Soc.* **126**, 2526 (2004).